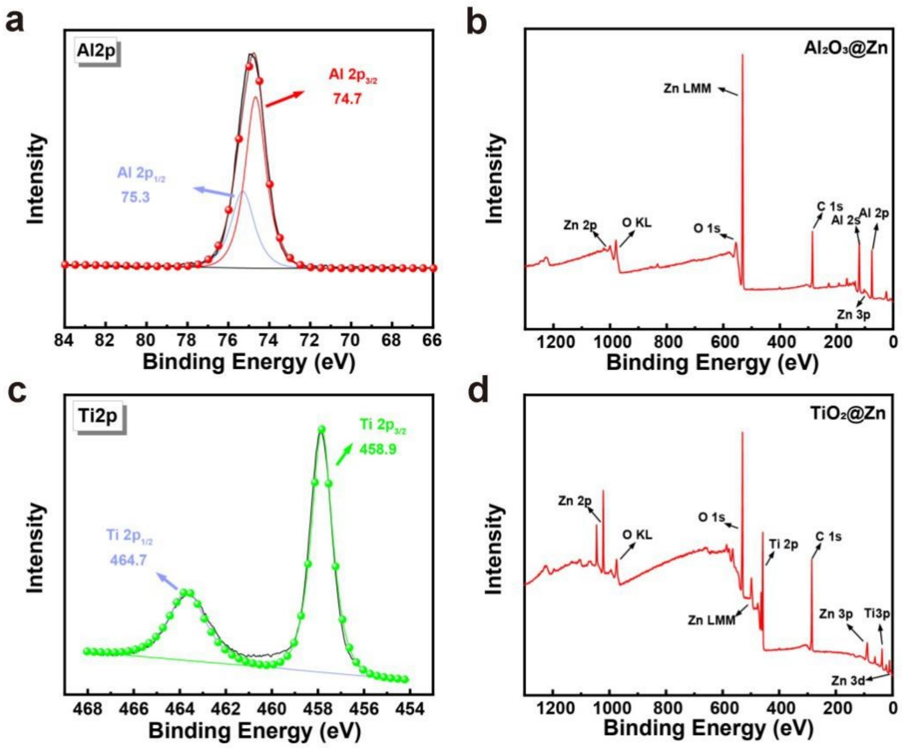

Fig. S1. XPS spectrum of a) Al 2p, b) full surveys before cycle for Al2O3@Zn and c) Ti 2p, d) full surveys before cycle for TiO2@Zn.

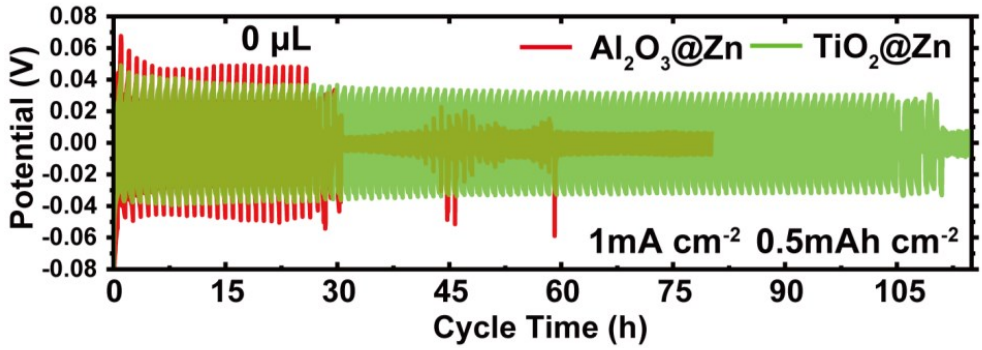

Fig. S2. Long-term symmetric tests of a) Al_2O_3@Zn, TiO_2@Zn without inducing sulfuric acid at a current density of 1 mA cm^{-2}.

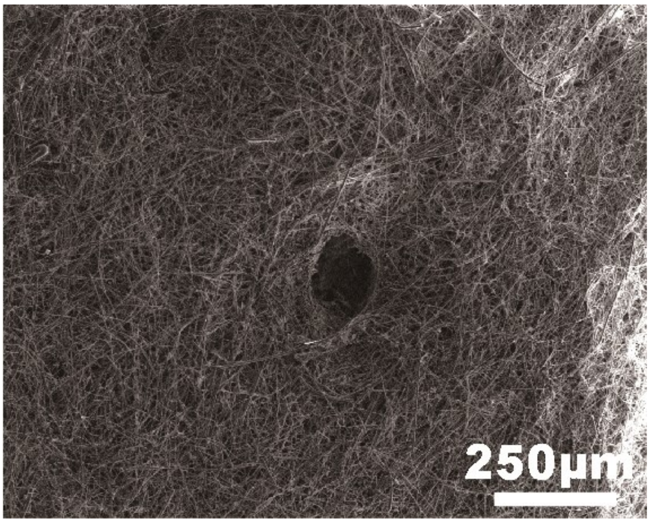

Fig. S3. The SEM image of glass fiber with an obvious pore structure penetrated by dendrite in Fe_2O_3@Zn-0 μL.

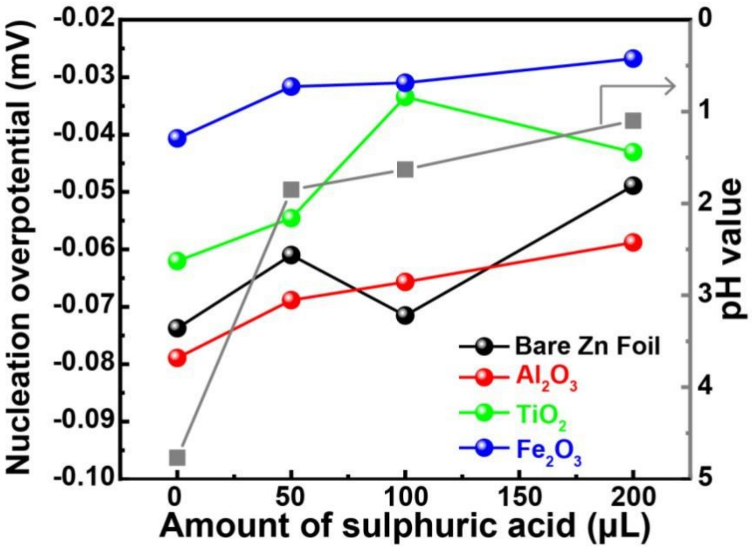

Fig. S4. The overpotentials of bare Zn foil and ALD@Zn with different electrolytes and corresponding pH value of different electrolytes. The pH values of electrolytes are 4.77, 1.85, 1.63 and 1.10 under 0, 50, 100 and 200 μL, respectively.

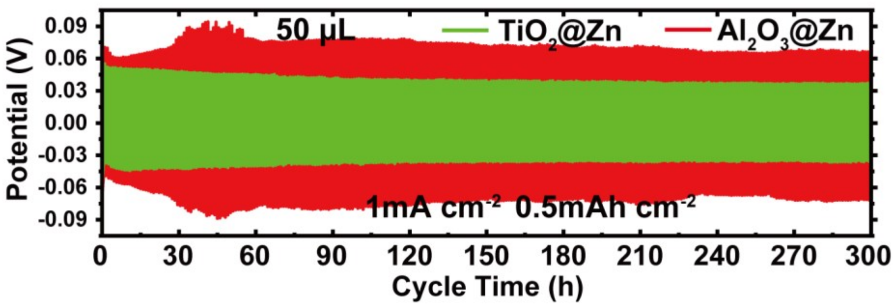

Fig. S5. Long-term symmetric tests of a)Al_2O_3@Zn, TiO_2@Zn within 50 μL sulfuric acid at a current density of 1 mA cm^{-2}.

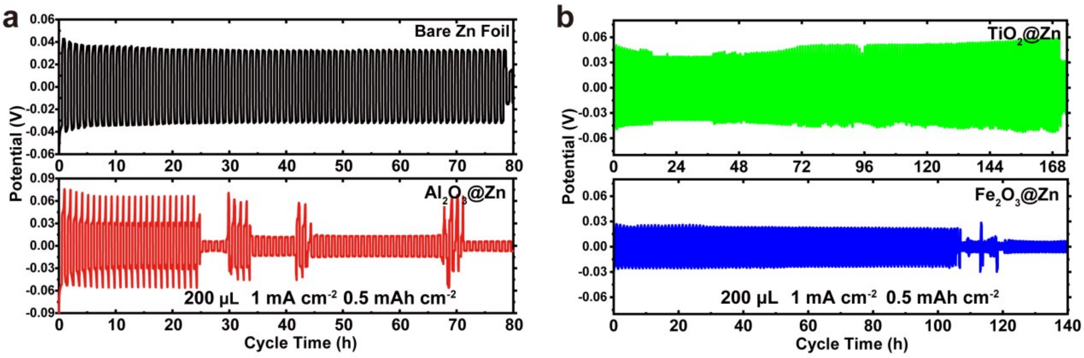

Fig. S6. Long-term symmetric tests of a)bare Zn foil, Al_2O_3@Zn, b) TiO_2@Zn and Fe_2O_3@Zn with 200 µL at a current density of 1 mA cm^{-2}.

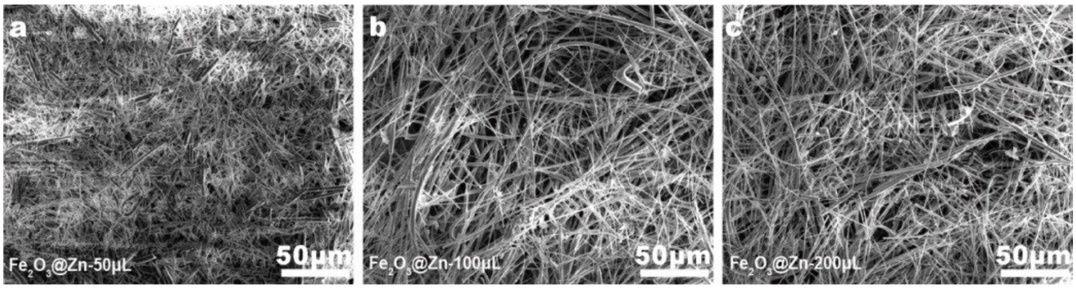

Fig. S7. SEM images of glass fiber after cycle in a) Fe_2O_3@Zn-50 µL, b) Fe_2O_3@Zn-100 µL, c) Fe_2O_3@Zn-200 µL at a current density of 1 mA cm^{-2}.

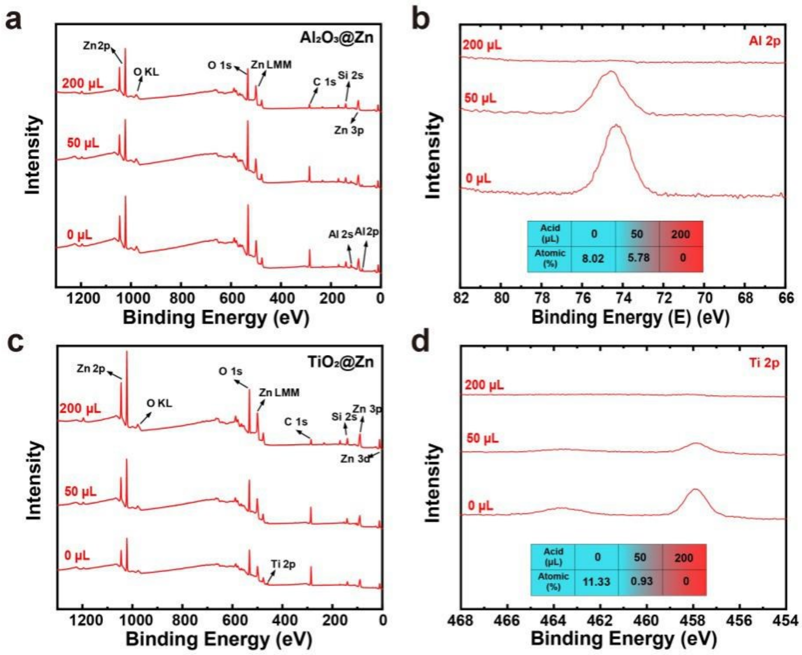

Fig. S8. XPS spectrum of a) surveys after cycling in 0, 50 and 200 µL and corresponding b) Al 2p on Al_2O_3@Zn; XPS spectrum of c) surveys after cycling in 0 and 50 and 200 µL and corresponding d) Ti 2p on TiO_2@Zn. The insets show Al 2p and Ti 2p peak table, respectively.

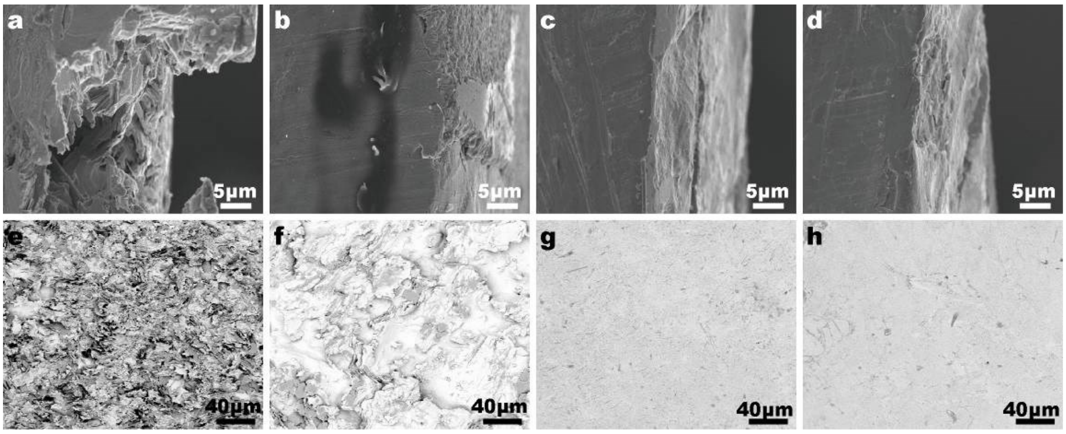

Fig. S9. Cross-sectional SEM images of a) bare Zn foil, b) Al_2O_3@Zn, c) TiO_2@Zn and d) Fe_2O_3@Zn after cycling at a current density of 0.1 mA cm^{-2}. SEM images of e) bare Zn foil, f) Al_2O_3@Zn, g) TiO_2@Zn and h) Fe_2O_3@Zn after cycling at a current density of 10 mA cm^{-2}.

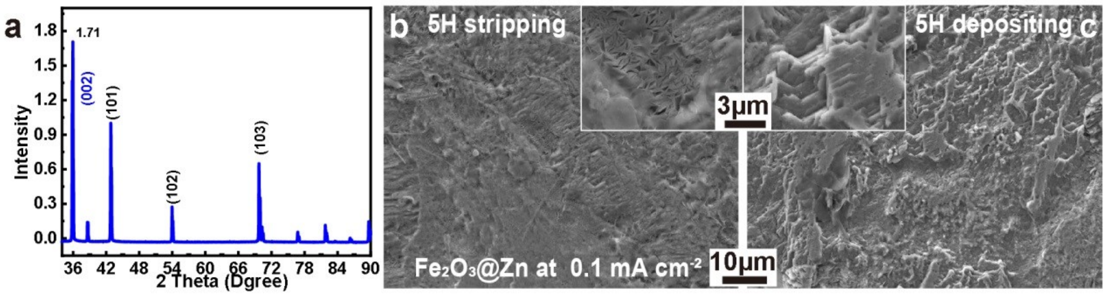

Fig. S10. a) XRD pattern of Fe_2O_3@Zn after 5 hours stripping at a current density of 0.1 mA cm^{-2} and corresponding b) SEM image. c) The texture on Fe_2O_3@Zn after 5 hours depositing at the same current.

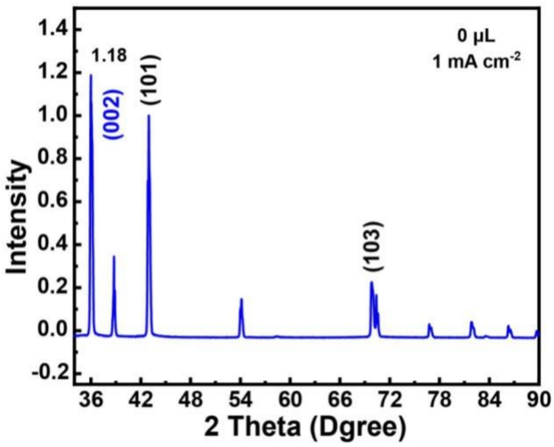

Fig. S11. XRD patterns of Fe_2O_3@Zn after depositing without inducing H^+ in the electrolyte.

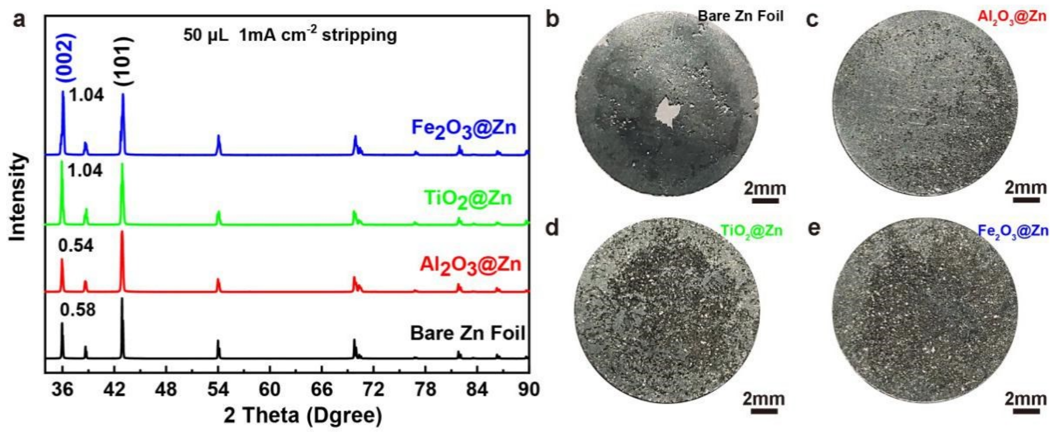

Fig. S12. a) XRD patterns of Zn after stripping and corresponding optical images of b) bare Zn foil, c) Al_2O_3@Zn, d) TiO_2@Zn and e) Fe_2O_3@Zn at a current density of 1 mA cm^{-2}.

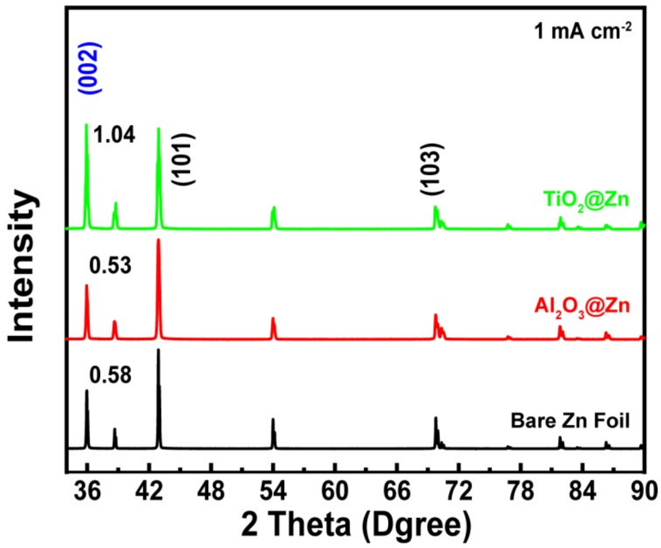

Fig. S13. XRD patterns of bare Zn foil, Al_2O_3@Zn, TiO_2@Zn after depositing.

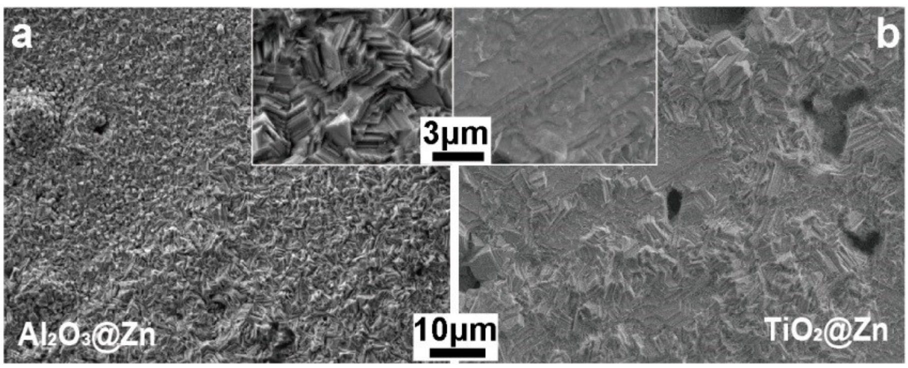

Fig. S14. SEM images of a) Al_2O_3@Zn and b) TiO_2@Zn after 5 hours depositing progress at a current density of 1 mA cm^{-2}.

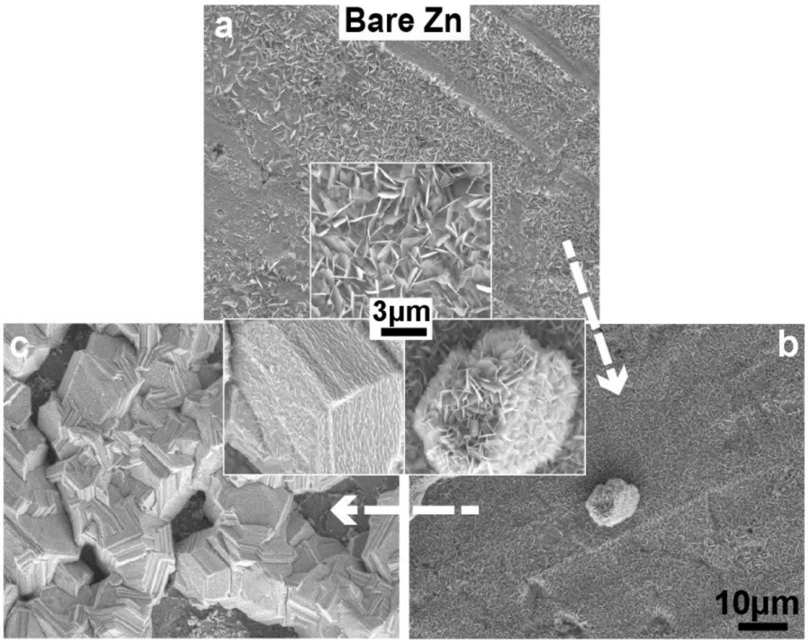

Fig. S15. a-c) SEM images of the growth evolution morphologies of favourable (101) orientation on bare Zn foil during depositing progress.

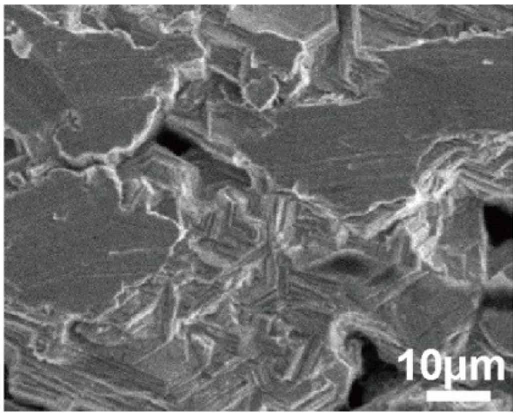

Fig. S16. SEM image of Fe_2O_3@Zn after depositing at a current density of 10 mA cm^{-2}.

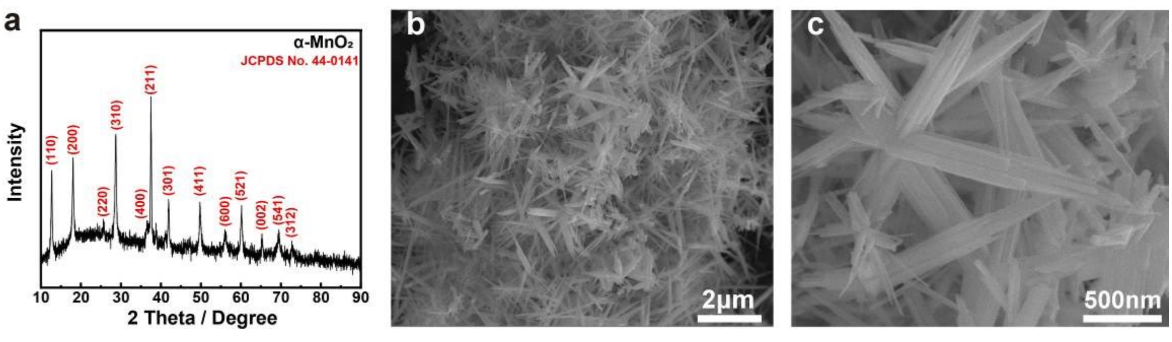

Figure S17. a) XRD pattern and b-c) SEM images of nanorod α-MnO_2.

Table S1. Summary comparison of electrochemical performance of Zn-MnO_2 batteries.

Cathod	Anode	Electrolyte	Capacity after fully activate (mAh g^{-1})	Cycle number	Capacity after cycle (mAh g^{-1})	Current density (A g^{-1})	Reference
α-MnO_2	**Fe_2O_3@Zn**	**3 M $ZnSO_4$ + 0.1 M $MnSO_4$+ H_2SO_2**	**280**	**1000**	**244.3**	**1**	**This work**
α-MnO_2	TiO_2@Zn	3 M $ZnSO_4$ + 0.1 M $MnSO_4$+ H_2SO_2	227.8	1000	192.6	1	This work
α-MnO_2	Al_2O_3@Zn	3 M $ZnSO_4$ + 0.1 M $MnSO_4$+ H_2SO_2	148.1	1000	147.2	1	This work
α-MnO_2	Zn@ZnO-3D	2 M $ZnSO_4$ + 0.1 M $MnSO_4$	226.5	500	212	0.5	1
δ-MnO_2	Al_2O_3@Zn	3 M $Zn(SO_3CF_3)_2$ + 0.1 M $Mn(SO_3CF_3)_2$	177.2	1000	158.4	1	2
α-MnO_2	TiO_2@Zn	3 M $Zn(SO_3CF_3)_2$ + 0.1 M $Mn(SO_3CF_3)_2$	<200	1000	134	1	3
CNT/MnO_2	nano-$CaCO_3$-coated Zn	3 M $ZnSO_4$ + 0.1 M $MnSO_4$	236	1000	177	1	4
CNT/MnO_2	Zn@ZnP	2 M $ZnSO_4$ + 0.1 M $MnSO_4$	<200	1000	154.4	1	5
δ-MnO_2	PPy-coated Zn	2 M $ZnSO_4$ + 0.1 M $MnSO_4$	≈200	200	≈175	1	6
MnO_2 NW	MOF-based Zn	2 M $ZnSO_4$ + 0.1 M $MnSO_4$	≈60	5000	≈50	0.308	7
α-MnO_2	3D Zn@Cu	2 M $ZnSO_4$ + 0.5 M $MnSO_4$	≈250	300	173	0.4	8
β-MnO_2	Zn@Cu foam	2 M $ZnSO_4$ + 0.1 M $MnSO_4$	≈210	600	173.8	1	9

1 X. Xie, S. Liang, J. Gao, S. Guo, J. Guo, C. Wang, G. Xu, X. Wu, G. Chen and J. Zhou, Energy Environ. Sci., 2020, **13**, 503-510.

2 H. He, H. Tong, X. Song, X. Song and J. Liu, J. Mater. Chem. A, 2020, **8**, 7836-7846.

3 K. Zhao, C. Wang, Y. Yu, M. Yan, Q. Wei, P. He, Y. Dong, Z. Zhang, X. Wang and L. Mai, Adv. Mater. Interfaces, 2018, **5**, 1800848.

4 L. Kang, M. Cui, F. Jiang, Y. Gao, H. Luo, J. Liu, W. Liang and C. Zhi, Adv. Energy Mater., 2018, **8**, 1801090.

5 P. Cao, X. Zhou, A. Wei, Q. Meng, H. Ye, W. Liu, J. Tang and J. Yang, Adv. Funct. Mater., 2021, **31**, 20, 2100398.

6 F. Zhang, C. Wang, J. Pan, F. Tian, S. Zeng, J. Yang and Y. Qian, Mater. Today Energy, 2020, 17, 100443.

7 R. Yuksel, O. Buyukcakir, W. K. Seong and R. S. Ruoff, Adv. Energy Mater., 2020, **10**, 1904215.

8 Z. Kang, C. Wu, L. Dong, W. Liu, J. Mou, J. Zhang, Z. Chang, B. Jiang, G. Wang, F. Kang and C. Xu, ACS Sustain. Chem. Eng., 2019, **7**, 3364-3371.

9 X. Shi, G. Xu, S. Liang, C. Li, S. Guo, X. Xie, X. Ma and J. Zhou, ACS Sustain. Chem. Eng., 2019, **7**, 17737-17746.